

Quadrupolar induced suppression of nuclear spin bath fluctuations in self-assembled quantum dots

E. A. Chekhovich¹, M. Hopkinson², M. S. Skolnick¹, and A. I. Tartakovskii¹

¹*Department of Physics and Astronomy, University of Sheffield, Sheffield S3 7RH, UK and*

²*Department of Electronic and Electrical Engineering,
University of Sheffield, Sheffield S1 3JD, UK*

(Dated: March 24, 2014)

Decoherence in quantum logic gates (qubits) due to interaction with the surrounding environment is a major obstacle to the practical realization of quantum information technologies. For solid state electron-spin qubits the interaction with nuclear spins is the main problem¹⁻⁷. One particular, ineradicable source of electron decoherence arises from decoherence of the nuclear spin bath, driven by nuclear-nuclear dipolar interactions. Due to its many-body nature nuclear decoherence is difficult to predict^{8,9}, especially for an important class of strained nanostructures where nuclear quadrupolar effects have a significant but largely unknown impact¹⁰. Here we report direct measurement of nuclear spin bath coherence in individual strained InGaAs/GaAs quantum dots: nuclear spin-echo coherence times in the range $T_2 \approx 1.2 - 4.5$ ms are found. Based on these T_2 values we demonstrate that quadrupolar interactions make nuclear fluctuations in strained quantum dots much slower compared to lattice matched GaAs/AlGaAs structures². Such fluctuation suppression is particularly strong for arsenic nuclei due to the effect of atomic disorder of gallium and indium alloying. Our findings demonstrate that quadrupolar effects can help to solve the long-standing challenge of designing a scalable hardware for quantum computation: III-V semiconductor spin-qubits can be engineered to have a noise-free nuclear spin bath (previously achievable only in nuclear spin-0 semiconductors¹¹⁻¹³, where qubit network interconnection and scaling is challenging).

Quantum dots in III-V semiconductors have many favourable properties for applications in quantum information processing including strong interaction with light offering excellent optical interfacing, manipulation at ultrafast speeds and advanced manufacturing technology^{2,4,5,14}. However, all atoms of groups III and V have nonzero nuclear magnetic moments. Thus instead of an ideal two-level quantum system, the spin of a single electron in a quantum dot is described by the so called "central spin" problem^{8,9,15}, where the electron (central) spin is subject to magnetic interaction with an ensemble of $10^4 - 10^6$ nuclear spins. This hyperfine interaction results in decoherence, i.e. decay of the phase information encoded in electron spin^{2,8,9,15}.

Hyperfine induced decoherence can be greatly reduced by applying static magnetic field and refocusing control pulses inducing electron spin echo. With this technique very long electron qubit coherence times of ~ 200 μ s were demonstrated in lattice matched GaAs/AlGaAs quantum dots². However, the effect of nuclei can not be eliminated completely due to presence of nuclear-nuclear (dipole-dipole) magnetic interactions, which cause spin exchange flip-flops of nuclei, i.e. nuclear spin bath decoherence. Due to the many-body nature of the nuclear spin bath such flip-flops

induce quasi-random fluctuating magnetic fields acting on electron spin and causing its decoherence ("spectral diffusion" process^{8,9,16}). It is thus evident that understanding the nuclear spin coherence is crucial for predicting the coherence properties of the central spin. Furthermore, strained quantum dots exhibit large nuclear quadrupolar interactions (QI)¹⁷. It is predicted that the QI can suppress the nuclear flip-flops resulting in extended electron spin coherence¹⁸. However, this possibility is little explored¹⁰, mainly due to the lack of reliable data on nuclear spin coherence in self-assembled dots.

Here we develop experimental techniques enabling pulsed nuclear magnetic resonance (NMR) of as few as $10^4 - 10^5$ quadrupolar spins in individual strained InGaAs/GaAs quantum dots. We probe nuclear coherence by measuring the spin-echo decay times T_2 , found to range from ~ 1.2 ms [for ^{71}Ga] to 4.5 ms [for ^{75}As], which is a factor of ~ 5 longer compared to unstrained GaAs/AlGaAs structures – a direct evidence of the nuclear spin flip-flop suppression. We then show that the nuclear flip-flop times $T_{2,ff}$ (relevant for electron spin decoherence) differ from spin-echo T_2 times, but can be estimated using a first-principle model¹⁹. For gallium and indium the strain-induced inhomogeneous QI results in $T_{2,ff} \sim 5$ ms, a factor of $\sim 3 - 8$ increase compared to lattice-matched structures. By contrast, for arsenic a much stronger flip-flop suppression is found ($T_{2,ff} \gg 5$ ms), an effect explained by additional inhomogeneous QI arising from random alloy mixing of gallium and indium atoms²⁰. Such atomic-scale disorder opens a new prospect for using the excellent properties of III-V quantum dots to build nuclear-spin-noise free solid-state qubits: This can now be done without resorting to materials with zero nuclear spin (e.g. isotopically pure ^{28}Si and ^{12}C)^{11–13}, which have inferior optical properties, hampering on-chip integration of a large number of qubits.

Our experiments were performed on individual neutral quantum dots in InGaAs/GaAs samples, grown by strain-driven self-assembly using molecular beam epitaxy. The sample was placed in an optical helium-bath cryostat ($T=4.2$ K). Magnetic field B_z up to 8 T was applied parallel to the sample growth axis (Oz) and light propagation direction (Faraday geometry). The structures were investigated using optically detected nuclear magnetic resonance (ODNMR) techniques which extend the concepts reported in our recent work^{17,21}. Radio-frequency (rf) fields B_{rf} perpendicular to B_z are induced by a minicoil wound around the sample (see further details in Methods and Supplementary Sections S1 and S2).

In this work we study the four most abundant isotopes: ^{69}Ga , ^{71}Ga , ^{75}As (spin $I = 3/2$) and ^{115}In (spin $I = 9/2$), all possessing non-zero quadrupolar moments. The proportion of Ga/In in our dots is estimated as 0.76/0.24 (Ref.¹⁷). The energy level diagram of a quadrupolar nuclear spin is shown schematically in Fig. 1(a) for the case of $I = 3/2$. Magnetic field B_z induces shifts

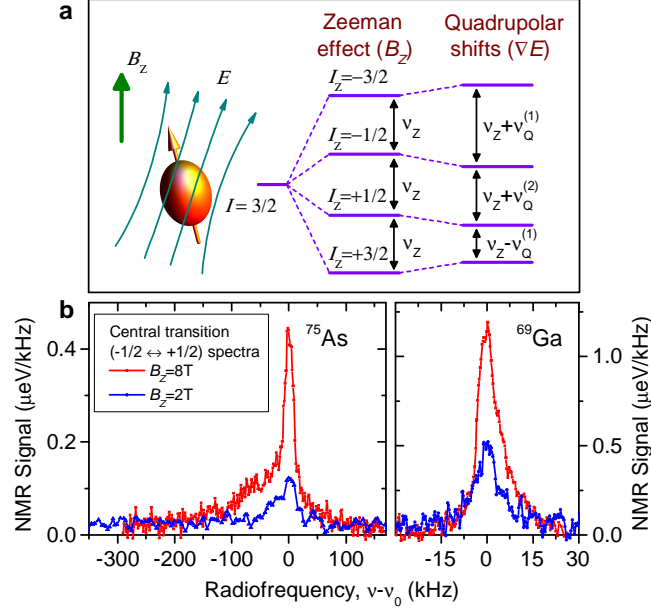


FIG. 1. **Nuclear quadrupolar effects in strained quantum dots.** **a**, Schematic representation of a half-integer quadrupolar nuclear spin ($I = 3/2$ is used as an example) and its energy spectrum. Magnetic field B_z splits the spin state into a Zeeman ladder, with dipole-allowed NMR transitions $I_z \leftrightarrow I_z \pm 1$ occurring at the same Larmor frequency ν_Z . Due to nonzero quadrupolar moment the electric field gradient $\nabla \vec{E}$ (induced e.g. by strain) causes first and second order NMR frequency shifts $\nu_Q^{(1)}, \nu_Q^{(2)}$ with $\nu_Q^{(1)} \gg \nu_Q^{(2)}$. **b**, Central transition spectra of ^{69}Ga and ^{75}As measured in an InGaAs QD using continuous wave "inverse" techniques¹⁷ at $B_z = 2$ and 8 T. At lower magnetic field the resonance peaks become weaker and broader, confirming that the linewidth is determined by the second order shifts $\nu_Q^{(2)} \propto 1/B_z$.

proportional to $\propto I_z$, so that all dipole-allowed NMR transitions ($\Delta I_z = \pm 1$) appear at the same frequency ν_Z . Electric field gradients $\nabla \vec{E}$ induce further shifts $\propto I_z^2$ to first order of perturbation²². The resulting NMR frequency shifts $\nu_Q^{(1)}$ are strongly inhomogeneous and are on the order of few MHz in InGaAs dots¹⁷. The central transition (CT) $-1/2 \leftrightarrow +1/2$ is an exception, since it is affected by QI only to second order resulting in much smaller shifts $\nu_Q^{(2)}$ on the order of tens to hundreds of kHz²². The relatively small linewidths greatly simplify the experiments; thus in what follows we focus on spectroscopy of CTs only. In particular, selective pulsed NMR of CTs can be conveniently implemented by choosing the rf amplitude B_{rf} so that $\nu_Q^{(2)} \lesssim \gamma B_{rf}/(2\pi) \ll \nu_Q^{(1)}$ (γ is the nuclear gyromagnetic ratio).

Fig. 1(b) shows CT spectra of ^{75}As and ^{69}Ga measured using continuous-wave "inverse" NMR techniques¹⁷. At high field $B_z = 8\text{ T}$ the ^{69}Ga resonance consists of a single narrow line (FWHM $\sim 9\text{ kHz}$). The arsenic resonance consists of a narrow line (FWHM $\sim 30\text{ kHz}$) and additional

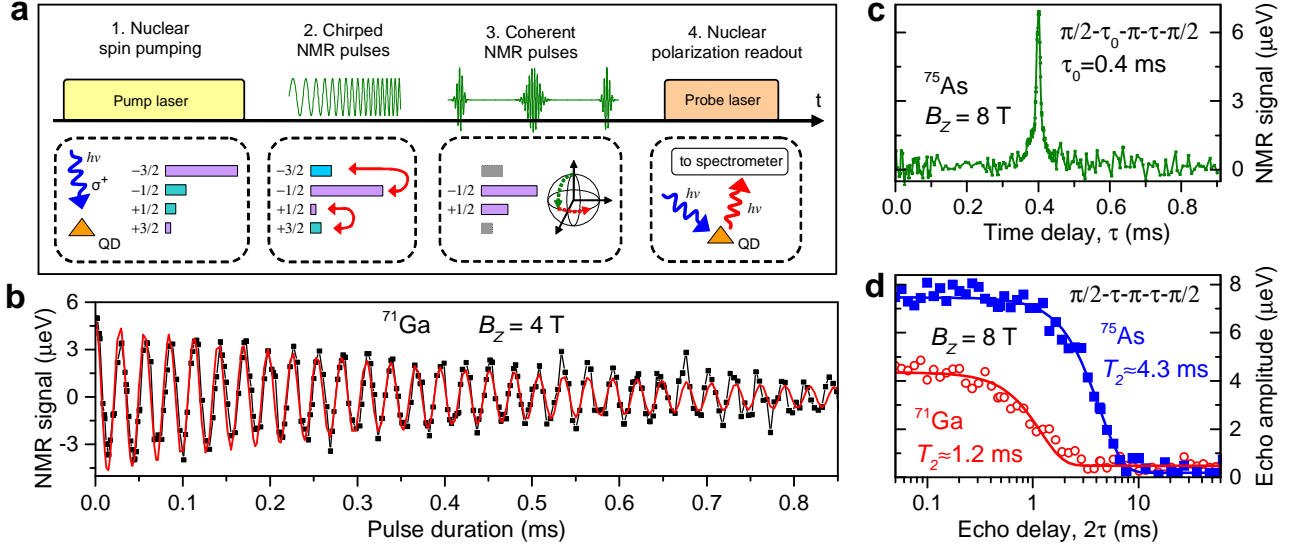


FIG. 2. **Pulsed NMR on central transitions ($-1/2 \leftrightarrow +1/2$) of quadrupolar nuclear spins in InGaAs quantum dots.** **a**, Experimental cycle timing consisting of four stages: (1) Optical pumping of a large ($>50\%$) nuclear spin polarization^{21,23}, (2) enhancement of the CT signal by chirped radiofrequency pulses via population transfer²⁴, (3) an arbitrary sequence of radiofrequency pulses selectively exciting the CT, (4) optical readout of the final nuclear spin polarization using hyperfine shifts in a photoluminescence spectrum^{21,23}. **b**, Rabi oscillations measurement (a single rf pulse of a variable duration). **c**, Hahn-echo measurement ($\pi/2 - \tau_0 - \pi - \tau - \pi/2$ sequence with $\tau_0 = 0.4 \text{ ms}$): a pronounced spin echo signal is observed at $\tau = 0.4 \text{ ms}$. **d**, Echo decay measurements at $B_z = 8 \text{ T}$ on ^{71}Ga (circles) and ^{75}As (squares): Spin echo amplitude is plotted as a function of the total delay 2τ of the $\pi/2 - \tau - \pi - \tau - \pi/2$ sequence. Lines show Gaussian decay fitting $\propto \exp(-(2\tau)^2/T_2^2)$ with decay times T_2 characterizing the nuclear spin coherence.

asymmetric "wings" stretching up to approximately $-150/+50 \text{ kHz}$. When magnetic field is reduced down to 2 T both resonances broaden and diminish in amplitude, as expected for a lineshape determined by second order quadrupolar shifts $\nu_Q^{(2)}$ (Ref.²²). The significantly larger broadening of the ^{75}As CT resonance is attributed to random intermixing of the group-III Ga and In atoms creating additional low-symmetry electric field gradients at arsenic sites^{17,20}. As we demonstrate below such random quadrupolar shifts result in pronounced suppression of dipolar nuclear flip-flops and extension of nuclear spin coherence times.

The quadrupolar broadening of NMR spectra in Fig. 1(b) is inhomogeneous in character. It obscures the much weaker homogeneous broadening induced by the nuclear-nuclear interactions which determine the nuclear spin coherence. In order to access the nuclear spin coherence we use time-domain (pulsed) NMR²²: the timing diagram of the pulsed NMR experiment is shown in Fig.

2(a) (further details on techniques can be found in Methods and Supplementary Section S2). We start with a Rabi nutation experiment where a single rf pulse of a variable duration τ is applied²⁵. Rabi oscillations of nuclear polarization are clearly seen in Fig. 2(b) enabling the calibration of $\pi/2$ and π rotation pulses. The decay of Rabi oscillations is due to dephasing caused by inhomogeneous spectral broadening [Fig. 1(b)]. Such dephasing can be reversed using the Hahn echo sequence $\pi/2 - \tau_0 - \pi - \tau - \pi/2$. The result of a measurement with a fixed delay $\tau_0 = 0.4$ ms and a variable τ are shown in Fig. 2(c) where as expected a pronounced spin echo is observed at $\tau = \tau_0$.

We then turn to the spin-echo decay measurements ($\pi/2 - \tau - \pi - \tau - \pi/2$ pulse sequence) where the evolution times τ before and after the π refocusing pulse are varied simultaneously. Figure 2(d) shows experimentally measured nuclear spin-echo amplitudes (symbols) as a function of the total delay time 2τ for ^{71}Ga and ^{75}As isotopes at $B_z = 8$ T. Experimental curves are well fitted by a Gaussian decay function (solid lines) with characteristic $1/e$ decay time $T_2 \approx 1.18$ ms for ^{71}Ga and $T_2 \approx 4.27$ ms for ^{75}As . The spin-echo sequence removes the effect of inhomogeneous spectral broadening, with the echo decay caused solely by the nuclear-nuclear dipolar interactions²²: T_2 thus characterizes the coherence of the nuclear spin bath. We have repeated spin-echo measurements for all four studied isotopes at different magnetic fields B_z . The resulting coherence times T_2 (and corresponding decay rates $1/T_2$) are plotted in Fig. 3 by the circles. In addition we have verified the reproducibility of our results by measuring T_2 of ^{75}As for another six individual dots from the same sample (see Supplementary Sec. S3).

In order to examine the effect of QI on the nuclear spin bath coherence we first compare our experimental T_2 times with previous nuclear spin echo measurements on GaAs/AlGaAs quantum wells and dots. The data available for ^{75}As (selective echo on CT in quantum wells (QWs)^{26–28}) and ^{71}Ga (non-selective echo on QWs²⁹ and QDs²⁵) is shown in Fig. 3(b) by the triangles. It can be seen that the echo decay times in self-assembled QDs are a factor of $\sim 5 - 7$ larger compared to lattice matched structures. Such increase in T_2 is due to suppression of nuclear spin flip-flops and provides direct evidence for the slow down of nuclear spin bath fluctuations in the presence of spatially inhomogeneous QI.

In order to quantify the effect of QI on the nuclear spin bath dynamics we turn to more detailed analysis of our experimental results. At sufficiently large magnetic field along Oz (above a few mT) the interaction between any two nuclear spins I and J is described by the "truncated" dipole-dipole Hamiltonian²²:

$$\hat{H}_{dd} = \nu_{dd} \left[\hat{I}_z \hat{J}_z - \frac{1}{2} (\hat{I}_x \hat{J}_x + \hat{I}_y \hat{J}_y) \right], \quad (1)$$

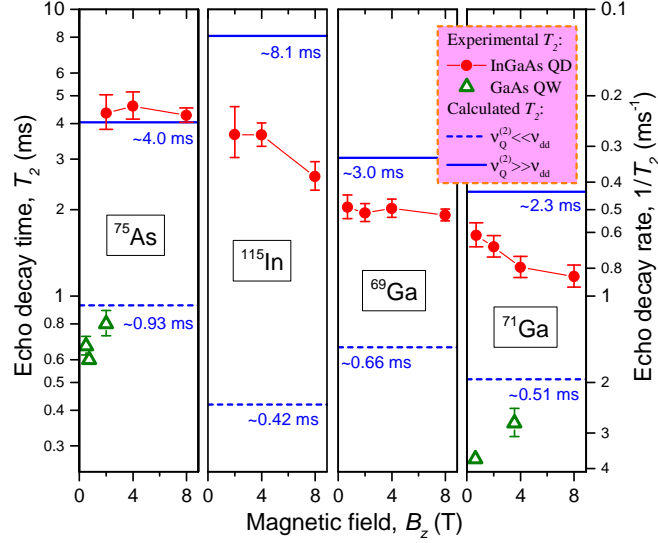


FIG. 3. **Nuclear spin-echo decay of central transitions.** Echo decay times T_2 (left scale) and corresponding decay rates $1/T_2$ (right scale) for four different isotopes as a function of B_z . Circles – experiment on strained InGaAs QDs (bars show 90% confidence intervals), triangles – measurements on lattice-matched GaAs/AlGaAs quantum wells (QWs) and QDs (data taken from Refs.^{25–29}). Calculated T_2 values¹⁹ are shown for the case of negligible second order quadrupolar shifts $\nu_Q^{(2)} \ll \nu_{dd}$ as in lattice matched GaAs/AlGaAs structures (dashed lines), and for the case of large inhomogeneous second order quadrupolar shifts $\nu_Q^{(2)} \gg \nu_{dd}$ resulting in complete suppression of nuclear flip-flops (solid lines).

where \hat{I} and \hat{J} are the spin operators, and the coupling strength ν_{dd} depends on nuclei type and mutual position ($\nu_{dd} \lesssim 200$ Hz in frequency units for nearest neighbors in InGaAs, and scales as $\propto r^{-3}$ with internuclear distance r). The $(\hat{I}_x\hat{J}_x + \hat{I}_y\hat{J}_y)$ term enables spin exchange flip-flops between nuclei I and J : $(I_z, J_z) \leftrightarrow (I_z \pm 1, J_z \mp 1)$, the process ultimately responsible for electron spin decoherence via spectral diffusion. A flip-flop can only happen if I and J have similar Zeeman energies requiring them to be of the same isotope. If, however, these two nuclei are subject to significantly different quadrupolar shifts $\nu_{Q,I}$ and $\nu_{Q,J}$, so that $|\nu_{Q,I} - \nu_{Q,J}| \gg \nu_{dd}$ the flip-flops will become energetically forbidden, resulting in a slow down of nuclear spin bath dynamics and potential increase in electron qubit coherence time¹⁸.

Despite the very simple structure of the Hamiltonian of Eq. S1, the calculation of the nuclear spin bath dynamics in a crystal is a very difficult task due to the many-body nature of the problem (each nuclear spin interacts with all other spins). When arbitrary inhomogeneous QI is added the problem becomes unsolvable in practice. However, for the limiting cases of very small and very large QI the nuclear spin echo decay times can be calculated with $\sim 25\%$ accuracy from the first principles using the method of moments¹⁹. The details of the calculation techniques are discussed

in the Methods and further in Supplementary Sec. S4; in what follows we present the results of these calculations and use them to analyze the experimental data.

When quadrupolar shifts are much smaller than the dipolar interaction $\nu_Q^{(2)} \ll \nu_Q^{(1)} \ll \nu_{dd}$, the nuclear flip-flops are not affected by QI. The T_2 times calculated for that case are shown in Fig. 3 with dashed lines for different isotopes. These calculated values are in good agreement with experiments on lattice matched GaAs/AlGaAs structures, confirming the validity of the model employed.

In the opposite case of very strong inhomogeneous QI $\nu_Q^{(1)} \gg \nu_Q^{(2)} \gg \nu_{dd}$ the dipole-dipole flip-flops become energetically forbidden. This effect can be described by truncating the flip-flop term in Eq. S1, leaving only the diagonal $\hat{I}_z \hat{J}_z$ term in the Hamiltonian. The $\hat{I}_z \hat{J}_z$ term conserves the nuclear polarization along the Oz axis. But for polarization orthogonal to Oz (as is in a spin-echo experiment after the initial $\pi/2$ pulse) this term causes decoherence³⁰, resulting in nuclear spin echo decay¹⁹ on a timescale which we denote as $T_{2,zz}$. The $T_{2,zz}$ times calculated for the studied InGaAs dots are shown by the solid lines in Fig. 3. The $T_{2,zz}$ sets an upper limit on the echo decay time T_2 .

We now turn to the question of how nuclear spin T_2 measurements can be used to predict the effect of the nuclear spin bath fluctuations on electron spin coherence. If the nuclear flip-flops were completely suppressed the electron spin would experience only a static nuclear field which cannot cause irreversible electron spin decoherence – a very attractive scenario for applications of quantum dots in quantum information processing. But as explained above the nuclear spin-echo T_2 time in that case does not tend to infinity, it rather tends to a finite maximum value given by $T_{2,zz}$. Thus in order to establish how strong the flip-flop suppression is, we examine how close the experimental T_2 value is to the calculated $T_{2,zz}$. For that we introduce a characteristic nuclear spin flip-flop time $T_{2,ff}$ defined as

$$T_{2,ff}^{-1} = T_2^{-1} - T_{2,zz}^{-1}, \quad (2)$$

so that in a quantum dot with $T_{2,ff} \rightarrow \infty$ we would expect electron spin coherence not limited by nuclear spins.

It can be seen in Fig. 3 that $T_2 < T_{2,zz}$ for In and both Ga isotopes implying only a partial suppression of the nuclear spin flip-flops. Using Eq. S7 we calculate $T_{2,ff} \sim 5$ ms for all three of those isotopes at low fields ($B_z < 2$ T). This $T_{2,ff}$ is $\sim 3 - 8$ times larger than it would have been in InGaAs/GaAs structures without strain ($T_{2,ff}$ values for this case are calculated to be $T_{2,ff} \sim 0.6$ ms, 1.5 ms, 1.1 ms for ^{115}In , ^{69}Ga and ^{71}Ga , see details in Supplementary Section S4).

We also note that the T_2 of ^{71}Ga and ^{115}In decreases with increasing B_z in agreement with the fact that second order quadrupolar shifts depend on magnetic field as $\nu_Q^{(2)} \propto 1/B_z$ (Ref.²²), so that large B_z re-enables the nuclear flip-flops between the $I_z = \pm 1/2$ spin states.

A very different picture is observed in Fig. 3 for arsenic nuclei: the values of T_2 measured at $B_z = 2 - 8$ T coincide with the calculated $T_{2,zz}$ within the experimental error. Eq. S7 in that case diverges and gives infinitely large $T_{2,ff}$ values, but we can conclude that $T_{2,ff} \gg 5$ ms for arsenic, implying very strong flip-flop suppression. These findings are consistent with the spectroscopic data in Fig. 1 (b), where the CT spectra of ^{75}As are found to be ~ 10 times broader than for gallium nuclei, revealing much larger second order quadrupolar shifts of arsenic nuclei, which are responsible for the strong suppression of the nuclear spin exchange flip-flops.

The second order shifts $\nu_Q^{(2)}$ appear whenever $\nabla \vec{E}$ is not a cylindrically-symmetric tensor with its main axis along B_z (Ref.²²). One obvious reason for low-symmetry $\nabla \vec{E}$ in self-assembled QDs, is non-uniaxial symmetry of the elastic strain tensor, or deviation of the strain main axis from B_z . Such a mechanism is likely to be the main cause of the CT inhomogeneous broadening of gallium and indium, resulting in the above increase in $T_{2,ff}$ by a factor of $\sim 3 - 8$.

For the anion ^{75}As additional $\nu_Q^{(2)}$ shifts are induced by random alloy mixing of the cationic Ga and In atoms: Each arsenic nucleus has four nearest neighbors, and unless all of them are of the same type (all gallium or all indium) a non-zero $\nabla \vec{E}$ will appear²⁰. Furthermore, unlike the elastic strain fields that change gradually over many crystal unit cells, the configuration of the neighboring atoms is random, so that even the nearest arsenic nuclei (which have the strongest dipolar coupling) can have very different $\nu_Q^{(2)}$. Such compositional disorder can induce large spatially inhomogeneous CT frequency shifts, drastically suppressing the flip-flops. We propose that such effects can be used to engineer QDs with a frozen nuclear spin bath. One possible approach is to substitute some of the arsenic nuclei with antimony and/or phosphorus: in such InGaAsSb(P) quantum dots gallium and indium spins will also experience large inhomogeneous $\nu_Q^{(2)}$ shifts due to atomic-scale alloy disorder, resulting in an overall slow down of the flip-flops for all isotopes.

The increase of the nuclear spin-echo T_2 observed for the central transitions is driven by the second order quadrupolar shifts $\nu_Q^{(2)}$ which are significantly smaller than the first order shifts $\nu_Q^{(1)}$ ($\nu_Q^{(2)} \sim 10 - 100$ kHz compared to $\nu_Q^{(1)} \sim 1 - 10$ MHz). Therefore, we expect that the flip-flops of the nuclei in $|I_z| > 1/2$ states (affected by $\nu_Q^{(1)}$) are effectively frozen for all isotopes in strained InGaAs dots. Consequently, electron spin decoherence in self-assembled dots is caused solely by the flip-flops of the nuclei in $I_z = \pm 1/2$ states.

Finding an exact relation between the nuclear spin bath coherence times and the central spin co-

herence times is a complicated problem, in particular when quadrupolar interactions are involved¹⁰. However, some general qualitative conclusions can be readily drawn. Firstly, it has been shown that for quantum dots the spectral diffusion is well into the "slow bath" regime (as opposed to "motional narrowing")⁸, thus the extended nuclear spin coherence times reported here are expected to result in longer central spin coherence times. Secondly, dynamic nuclear spin polarization²³, that enhances the occupancy of the $|I_z| \approx I$ states can be used to effectively depopulate and "dilute" the $I_z = \pm 1/2$ states resulting in further reduction of the nuclear spin fluctuations. Based on recent observation of electron spin coherence times $> 200 \mu\text{s}$ in lattice matched GaAs/AlGaAs QDs², we may anticipate even longer, millisecond-range coherence times for self-assembled InGaAs/GaAs dots.

In conclusion we have demonstrated the first direct probing of the coherent nuclear spin bath dynamics in strained quantum dots. We predict that electron spin qubits in self-assembled structures exhibiting large quadrupolar interactions have a significant advantage over the lattice-matched counterparts. Engineering of strain and alloy disorder can be used to enhance this advantage further and open the way for optically-active quantum dot qubits with completely frozen nuclear spin environment. Future progress in this direction will depend strongly on advances in theoretical modeling of the central spin coherence in presence of quadrupolar effects¹⁰, a problem which previously could not be fully grasped due to the lack of experimental knowledge on the nuclear spin coherence. The techniques for pulsed NMR in strained quantum dots developed here are not restricted to spin-echo and can be readily extended to accommodate the whole variety of pulse sequences used in Fourier transform NMR, offering a powerful tool to explore the many-body physics of interacting nuclear spins in strained nanostructures.

METHODS SUMMARY

Continuous wave NMR spectroscopy. The CT spectra of an individual InGaAs/GaAs QD shown in Fig. 1(b) were measured using "inverse" method which provides >8 times CT signal enhancement for $I = 3/2$ nuclei¹⁷. The NMR signal is calculated as the hyperfine shift of the quantum dot Zeeman doublet divided by the spectral "gap" width, so that the values on the vertical scale give the spectral density of the distribution of the nuclear resonance frequencies. The spectral gap width (determining the spectral resolution) is 6 kHz for the ^{69}Ga spectra, and 16 kHz (32 kHz) for the $B_z = 8 \text{ T}$ ($B_z = 2 \text{ T}$) spectrum of ^{75}As . For convenience the spectra are plotted as a function of $\nu - \nu_0$, where ν_0 is a constant proportional to the isotope gyromagnetic ratio:

$\nu_0/B_z \approx 7.33$ MHz/T for ^{75}As and $\nu_0/B_z \approx 10.3$ MHz/T for ^{69}Ga .

Techniques for pulsed NMR measurements. We implement optically detected pulsed NMR techniques which extend the techniques and are based on the results of our previous work of Ref.¹⁷. The timing diagram of one measurement cycle and the changes to nuclear spin polarization are shown schematically in Fig. 2(a) (spin $I = 3/2$ is used as an example). The cycle starts with optical pumping using high power σ^+ circularly polarized laser [stage (1)]. Spin polarized electrons excited by the laser transfer their polarization to nuclear spins via the hyperfine interaction^{21,23}. Pump duration is chosen long enough ($\sim 3 - 7$ s depending on magnetic field B_z) to achieve the steady state nuclear spin polarization degrees exceeding 50%, which means that a large portion of the nuclei is initialized into the $I_z = -3/2$ state. In order to make the NMR signal of the central transition detectable the population of the $I_z = -1/2(+1/2)$ state must be maximized (minimized). This is done at stage (2) using "population transfer" technique²⁴: an rf field containing two frequency components is applied, the frequencies are swept over both satellite transition bands $-3/2 \leftrightarrow -1/2$ and $+1/2 \leftrightarrow +3/2$ resulting in adiabatic inversion of the populations of the $-3/2$ and $-1/2$ states as well as $+1/2$ and $+3/2$ states. Following that a sequence of rf pulses resonant with the CT is applied [stage (3)]. Different sequences can be implemented, depending on the experiment: a single pulse of a variable duration is used for Rabi-oscillation measurements [Fig. 2(b)], while a three-pulse sequence is used to measure either the spin-echo [Fig. 2(c), $\pi/2 - \tau_0 - \pi - \tau - \pi/2$ sequence with τ_0 fixed to 0.4 ms] or spin-echo decay [Fig. 2(d), $\pi/2 - \tau - \pi - \tau - \pi/2$ sequence]. The rf amplitude is chosen to give $\pi/2$ phase rotation for 3 - 8 μs long pulses (depending on isotope). This corresponds to pulse bandwidths of ~ 100 kHz, and, since satellite transitions are shifted by the much bigger ($\sim 1 - 10$ MHz) first order quadrupolar shifts, this ensures selective excitation of the central transition. Finally [stage (4)] we probe the effect of the NMR pulse sequence by measuring the changes in the average nuclear spin polarization $\langle I_z \rangle$ on the single quantum dot. This is achieved by exciting the dot with a short ($\sim 1 - 4$ ms depending on B_z) probe laser pulse and measuring the hyperfine shifts in the QD photoluminescence spectrum. In order to improve the signal to noise ratio the experimental cycle is repeated 20 - 50 times for each parameter value [e.g. for each value of 2τ in Fig. 2(d)]. Further details of experimental techniques can be found in Supplementary Sections S2.

Theoretical model. Nuclear spin decoherence is a result of nuclear-nuclear spin interactions: each individual nuclear spin has its own spin environment producing additional magnetic field, which changes the resonant frequency of that nucleus. Thus the problem of calculating the nuclear spin decoherence is equivalent to the problem of calculating homogeneous NMR line broadening.

In principle this problem can be solved by diagonalizing the Hamiltonian of the nuclear-nuclear interactions. This however is practically impossible even for a system of few tens of spins, let alone the whole crystal. An insightful solution to this difficulty has been found by Van Vleck^{22,31} who showed that the moments of the NMR lineshape can be expressed as traces of certain quantum mechanical operators. The key property of the trace is that it can be calculated in any wavefunction basis, hence diagonalization of the Hamiltonian is not needed. This technique does not allow an exact resonance lineshape to be found, but in most cases the second moment M_2 (corresponding to the homogeneous NMR linewidth) contains sufficient information.

The nuclear spin coherence time can be estimated as $T_2 \approx \sqrt{2/M_2}$. The calculation of M_2 for a whole crystal is a straightforward but very tedious process involving summation of various matrix elements. If one wants to calculate the spin-echo coherence time (as opposed to the free-induction decoherence time), some of the matrix elements must be discarded from the summation. Quadrupolar interaction is also taken into account by further "truncation" of the sums. The details of these calculations can be found in Refs.^{19,22,31} and are also outlined in Supplementary Sec. S4.

ACKNOWLEDGMENTS The authors are grateful to G. Burkard, E. Welander, L. Cywinski and K. V. Kavokin for fruitful discussion. This work has been supported by the EPSRC Programme Grant EP/J007544/1 and the Royal Society. E.A.C. was supported by a University of Sheffield Vice-Chancellor's Fellowship.

ADDITIONAL INFORMATION Correspondence and requests for materials should be addressed to E.A.C. (e.chekhovich@sheffield.ac.uk).

-
- ¹ Urbaszek, B., Marie, X., Amand, T., Krebs, O., Voisin, P., Maletinsky, P., Högele, A., and Imamoglu, A., Nuclear spin physics in quantum dots: An optical investigation. *Rev. Mod. Phys.* **85**, 79–133 (2013).
 - ² Bluhm, H., Foletti, S., Neder, I., Rudner, M., Mahalu, D., Umansky, V., and Yacoby, A., Dephasing time of GaAs electron-spin qubits coupled to a nuclear bath exceeding 200 us. *Nature Physics* **7**, 109 (2011).
 - ³ De Greve, K., McMahon, P. L., Press, D., Ladd, T. D., Bisping, D., Schneider, C., Kamp, M., Worschech, L., Hofling, S., Forchel, A., and Yamamoto, Y., Ultrafast coherent control and suppressed nuclear feedback of a single quantum dot hole qubit. *Nature Phys.* **7**, 872 (2011).
 - ⁴ Koppens, F. H. L., Buizert, C., Tielrooij, K. J., Vink, I. T., Nowack, K. C., Meunier, T., Kouwenhoven, L. P., and Vandersypen, L. M. K., Driven coherent oscillations of a single electron spin in a quantum dot. *Nature* **442**, 766 (2006).
 - ⁵ Pribyag, V. S., S., N.-P., Frolov, S. M., van den Berg, J. W. G., van Weperen, I., Plissard, S. R., Bakkers,

- E. P. A. M., and Kouwenhoven, L. P., Electrical control of single hole spins in nanowire quantum dots. *Nature Nanotech.* **8**, 170–174 (2013).
- ⁶ Greilich, A., Carter, S. G., Kim, D., Bracker, A. S., and Gammon, D., Optical control of one and two hole spins in interacting quantum dots. *Nature Photon.* **5**, 702–708 (2011).
 - ⁷ Kuhlmann, A. V., Houel, J., Ludwig, A., Greuter, L., Reuter, D., Wieck, A. D., Poggio, M., Warburton, R. J., Charge noise and spin noise in a semiconductor quantum device. *Nature Physics* **9**, 570–575 (2013).
 - ⁸ de Sousa, R. and Das Sarma, S., Theory of nuclear-induced spectral diffusion: Spin decoherence of phosphorus donors in Si and GaAs quantum dots. *Phys. Rev. B* **68**, 115322 (2003).
 - ⁹ Yao, W., Liu, R.-B., and Sham, L. J., Theory of electron spin decoherence by interacting nuclear spins in a quantum dot. *Phys. Rev. B* **74**, 195301 (2006).
 - ¹⁰ Sinitsyn, N. A., Li, Y., Crooker, S. A., Saxena, A., and Smith, D. L., Role of nuclear quadrupole coupling on decoherence and relaxation of central spins in quantum dots. *Phys. Rev. Lett.* **109**, 166605 (2012).
 - ¹¹ Saeedi, K., Simmons, S., Salvail, J. Z., Dluhy, P., Riemann, H., Abrosimov, N. V., Becker, P., Pohl, H.-J., Morton, J. J. L., and Thewalt, M. L. W., Room-temperature quantum bit storage exceeding 39 minutes using ionized donors in silicon-28. *Science* **342**, 830–833 (2013).
 - ¹² Laird, E. A., Pei, F., and Kouwenhoven, L. P., A valley-spin qubit in a carbon nanotube. *Nature Nanotech.* **8**, 565–568 (2013).
 - ¹³ Neumann, P., Kolesov, R., Naydenov, B., Beck, J., Rempp, F., Steiner, M., Jacques, V., Balasubramanian, G., Markham, M. L., Twitchen, D. J., Pezzagna, S., Meijer, J., Twamley, J., Jelezko, F., and Wrachtrup, J., Quantum register based on coupled electron spins in a room-temperature solid. *Nature Phys.* **6**, 249–253 (2010).
 - ¹⁴ Reilly, D. J., Taylor, J. M., Petta, J. R., Marcus, C. M., Hanson, M. P., and Gossard, A. C., Suppressing Spin Qubit Dephasing by Nuclear State Preparation. *Science* **321**, 817–821 (2008).
 - ¹⁵ Merkulov, I. A., Efros, A. L., and Rosen, M., Electron spin relaxation by nuclei in semiconductor quantum dots. *Phys. Rev. B* **65**, 205309 (2002).
 - ¹⁶ Witzel, W. M. and Das Sarma, S., Quantum theory for electron spin decoherence induced by nuclear spin dynamics in semiconductor quantum computer architectures: Spectral diffusion of localized electron spins in the nuclear solid-state environment. *Phys. Rev. B* **74**, 035322 (2006).
 - ¹⁷ Chekhovich, E. A., Kavokin, K. V., Puebla, J., Krysa, A. B., Hopkinson, M., Andreev, A. D., Sanchez, A. M., Beanland, R., Skolnick, M. S., and Tartakovskii, A. I., Structural analysis of strained quantum dots using nuclear magnetic resonance. *Nature Nanotech.* **7**, 646–650 (2012).
 - ¹⁸ Dzhioev, R. I. and Korenev, V. L., Stabilization of the electron-nuclear spin orientation in quantum dots by the nuclear quadrupole interaction. *Phys. Rev. Lett.* **99**, 037401 (2007).
 - ¹⁹ Haase, J. and Oldfield, E., Spin-echo behavior of nonintegral-spin quadrupolar nuclei in inorganic solids. *Journal of Magnetic Resonance, Series A* **101**, 30–40 (1993).
 - ²⁰ Knijn, P. J., van Bentum, P. J. M., van Eck, E. R. H., Fang, C., Grimminck, D. L. A. G., de Groot,

- R. A., Havenith, R. W. A., Marsman, M., Meerts, W. L., de Wijs, G. A., and Kentgens, A. P. M., A solid-state NMR and DFT study of compositional modulations in $\text{Al}_x\text{Ga}_{1-x}\text{As}$. *Phys. Chem. Chem. Phys.* **12**, 11517–11535 (2010).
- ²¹ Chekhovich, E. A., Glazov, M. M., Krysa, A. B., Hopkinson, M., Senellart, P., Lemaitre, A., Skolnick, M. S., and Tartakovskii, A. I., Element-sensitive measurement of the hole-nuclear spin interaction in quantum dots. *Nature Phys.* **9**, 74–78 (2013).
- ²² Abragam, A., *The Principles of Nuclear Magnetism*. Oxford University Press, London (1961).
- ²³ Gammon, D., Efros, A. L., Kennedy, T. A., Rosen, M., Katzer, D. S., Park, D., Brown, S. W., Korenev, V. L., and Merkulov, I. A., Electron and nuclear spin interactions in the optical spectra of single GaAs quantum dots. *Phys. Rev. Lett.* **86**, 5176–5179 (2001).
- ²⁴ Haase, J. and Conradi, M. S., Sensitivity enhancement for NMR of the central transition of quadrupolar nuclei. *Chemical Physics Letters* **209**, 287 – 291 (1993).
- ²⁵ Makhonin, M. N., Kavokin, K. V., Senellart, P., Lemaitre, A., Ramsay, A. J., Skolnick, M. S., and Tartakovskii, A. I., Fast control of nuclear spin polarization in an optically pumped single quantum dot. *Nature Materials* **10**, 848 (2011).
- ²⁶ Kondo, Y., Ono, M., Matsuzaka, S., Morita, K., Sanada, H., Ohno, Y., and Ohno, H., Multipulse operation and optical detection of nuclear spin coherence in a GaAs/AlGaAs quantum well. *Phys. Rev. Lett.* **101**, 207601 (2008).
- ²⁷ Ono, M., Sato, G., Ishihara, J., Matsuzaka, S., Ohno, Y., and Ohno, H., Nuclear spin coherence time in a strained GaAs quantum well. *AIP Conference Proceedings* **1399**, 685–686 (2011).
- ²⁸ Ishihara, J., Ono, M., Sato, G., Matsuzaka, S., Ohno, Y., and Ohno, H., Magnetic field dependence of quadrupolar splitting and nuclear spin coherence time in a strained (110) GaAs quantum well. *Japanese Journal of Applied Physics* **50**, 04DM03 (2011).
- ²⁹ Sanada, H., Kondo, Y., Matsuzaka, S., Morita, K., Hu, C. Y., Ohno, Y., and Ohno, H., Optical pump-probe measurements of local nuclear spin coherence in semiconductor quantum wells. *Phys. Rev. Lett.* **96**, 067602 (2006).
- ³⁰ The nuclear spin-echo decay due to the $\hat{I}_z\hat{J}_z$ term of the Hamiltonian can also be understood using the following simplified picture: The first $\pi/2$ rotation of the echo sequence transforms the initial I_z nuclear magnetization into I_x , which then evolves under the $\hat{I}_z\hat{J}_z$ Hamiltonian. This is equivalent to magnetization remaining in the I_z state while the Hamiltonian is transformed into $\hat{I}_x\hat{J}_x$, which is a flip-flop term that does not conserve nuclear polarization and causes echo decay.
- ³¹ Van Vleck, J. H., The dipolar broadening of magnetic resonance lines in crystals. *Phys. Rev.* **74**, 1168–1183 (1948).

SUPPLEMENTARY INFORMATION

The document consists of the following sections:

- S1. Quantum dot sample structure
- S2. Details of pulsed NMR techniques
 - S2 A. Pump-probe techniques for optically detected pulsed NMR
 - S2 B. Pulsed optically detected NMR: the hardware
- S3. Additional experimental results
- S4. First principle calculation of the nuclear spin-echo decay time T_2
 - S4 A. Nuclear spin echo decay under strongly inhomogeneous quadrupolar shifts [case (i)]
 - S4 B. Nuclear spin echo decay under homogeneous quadrupolar shifts [case (ii)]

S1. QUANTUM DOT SAMPLE STRUCTURE

The InGaAs/GaAs sample has been described previously in Refs.^{S1–S3} and in The Supplementary Information of Refs.^{S4,S5}. The sample consists of a single layer of nominally InAs quantum dots (QDs) placed within a microcavity structure which is used to select and enhance the photoluminescence from part of the inhomogeneous distribution of QD energies. The sample was grown by molecular beam epitaxy. The QDs were formed by deposition of 1.85 monolayers (MLs) of InAs - just above that required for the nucleation of dots. As a result, we obtain a low density of QDs at the post-nucleation stage. The cavity Q factor is ~ 250 and the cavity has a low temperature resonant wavelength at around 920 nm.

S2. DETAILS OF PULSED NMR TECHNIQUES

We implement optically detected pulsed NMR techniques which extend the techniques of our previous work^{S4,S5}. Some description of experimental techniques was previously reported in the Supplementary of Ref.^{S4} and also applies to this work. Below we focus on the techniques specific to the present work.

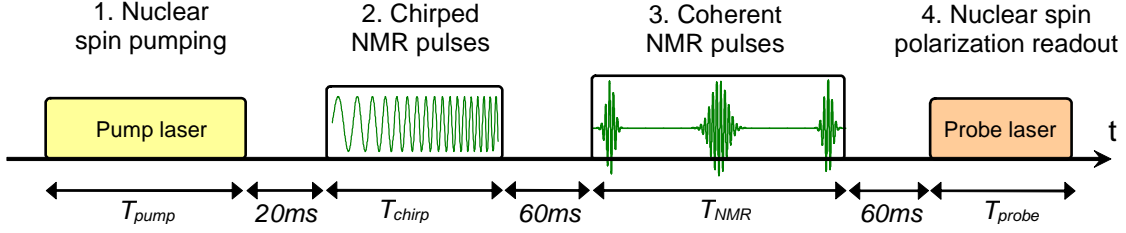


FIG. S1. **Timing diagram for pulsed NMR experiments on strained quantum dots.** See detailed explanation in Sec. S2 A.

A. Pump-probe techniques for optically detected pulsed NMR

The timing diagram of one measurement cycle is shown schematically in Fig. S1 (this is a detailed version of diagram in Fig. 2(a) of the main text). The cycle consists of the following four stages:

Stage 1. In order to achieve sufficiently large NMR signal the nuclei must be prepared in a highly-polarized state. Manipulation of nuclear spin polarization relies on the hyperfine interaction of electrons and nuclear spins. Excitation with a σ^+ circularly polarized "pump" laser generates spin polarized electrons, which transfer their polarization to nuclear spins via the hyperfine interaction^{S6–S11}. In this work dynamic nuclear spin polarization (polarization degrees exceeding 50%) is achieved using high power nonresonant optical pumping^{S3}. The pumping wavelength of ~ 850 nm corresponds to excitation into the QD wetting layer states. Optical powers exceeding the QD saturation level by more than a factor of 10 are typically used^{S3, S11}. At these powers the dependence of the steady-state nuclear polarization on the optical power saturates. This ensures large nuclear spin polarization degree as well as its good reproducibility due to insensitivity to laser power fluctuations. Pump durations of $T_{\text{pump}} = 3 - 7$ s (depending on magnetic field B_z) are used to achieve a steady-state polarization independent of the polarization left after the previous cycle. A delay of 20 ms is introduced after the pumping to ensure that the pump laser is completely blocked by a mechanical shutter, so that NMR on a quantum dot is measured in the dark.

Stage 2. The amplitude of the NMR signal of the central transition (CT) studied in this work is determined by the difference in population probabilities of the $I_z = -1/2$ and $I_z = +1/2$ nuclear spin states. However, for spin $I > 1/2$ inducing large nuclear spin polarization degree does not necessarily increase the CT signal. In fact, in the limit of 100% polarization all nuclei will be in the $I_z = -I$ state and the NMR signal of CT will vanish. Simple analysis shows that any optically induced (Boltzmann) distribution would yield CT NMR signal too weak to detect in

our setup. Thus nuclear spin level populations have to be manipulated artificially. We achieve this via "population transfer" techniques^{S12} which uses chirped radio-frequency (rf) pulses. For spin-3/2 nuclei we use an rf field containing two spectral components. The frequencies of both components are swept "outwards" from $\nu_{CT} \pm \nu_i$ to $\nu_{CT} \pm \nu_f$, where ν_{CT} is the frequency of the central transition. The initial frequency offset is chosen to be $\nu_i = 20$ kHz, whereas the final offset is chosen to be larger than the maximum first-order quadrupolar shift of the studied isotope ($\nu_f = 8.5$ MHz for ^{75}As , $\nu_f = 5.6$ MHz for ^{69}Ga and $\nu_f = 3.5$ MHz for ^{71}Ga are used). Such frequency sweeps adiabatically swap the populations of the $-3/2$ and $-1/2$ states as well as $+1/2$ and $+3/2$ states, significantly enhancing the population difference of the $\pm 1/2$ states. For spin-9/2 indium the sweeps are done "inwards" ($\nu_i > \nu_f$), with $\nu_i = 8.5$ MHz and $\nu_f = 120 - 230$ kHz, which effectively transfers the populations of the $\pm 9/2$ states to the $\pm 1/2$ states. The amplitude of each swept component is $\sim 0.2 - 0.5$ mT. The sweep rate is calibrated in an additional measurement and is chosen to maximize the CT signal. Typical rates used are $\sim 7 - 20$ MHz/s, so that the duration of the chirped pulse is $T_{chirp} \sim 0.3 - 1.5$ s. After the sweep a 60 ms delay is introduced to permit any transverse nuclear magnetization to decay and allow a mechanical relay to switch between the "chirp" and "pulse" rf signal sources (see Section S2B).

Stage 3. A sequence of rf pulses resonant with the central transition is applied to manipulate coherently the magnetization of the $I_z = \pm 1/2$ nuclear spin subspace. Different sequences can be implemented, e.g. Rabi-oscillations, Hahn-echo or echo decay, as demonstrated in Fig. 2 of the main text. The rf amplitude is chosen to give $\pi/2$ phase rotation of the $I_z = \pm 1/2$ subspace for 3-8 μs long pulse (depending on isotope). All pulse sequences are designed in a way that the final magnetization that needs to be measured is projected on to the Oz axis, so that it can be detected optically. For example in the echo decay sequence $\pi/2 - \tau - \pi - \tau - \pi/2$ the last $\pi/2$ pulse rotates the transverse magnetization (which is of interest) aligning it along the Oz axis. The total duration of the NMR pulse sequence T_{NMR} varies from a few microseconds to 110 ms. After the pulse sequence a 60 ms delay is introduced to allow the decay of any spurious transverse nuclear magnetization and the dissipation of heating induced by chirped or resonant NMR pulses.

Stage 4. Finally we probe the effect of the NMR pulse sequence by measuring the changes in the average nuclear spin polarization $\langle I_z \rangle$ on the dot. This is achieved by exciting the dot with a short ($T_{probe} = 1 - 4$ ms depending on B_z) nonresonant (~ 850 nm) probe laser pulse and measuring the hyperfine shifts of the Zeeman splitting in the QD photoluminescence spectrum^{S4-S6}. The power of the probe laser is $\sim 1/10$ of the QD saturation power. We use differential measurements: for spin-echo and echo decay experiments the NMR signal is calculated as the difference of the QD

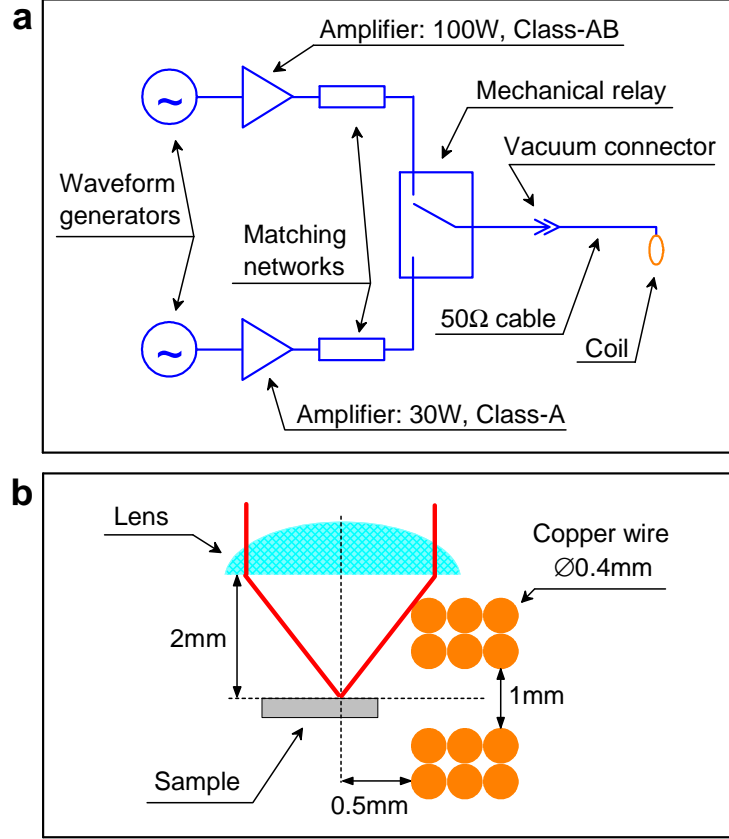


FIG. S2. **Hardware implementation of the pulsed NMR techniques.** **a**, Circuit diagram. **b**, Schematic drawing of the NMR coil arrangement (side view). See detailed explanation in Sec. S2 B.

Zeeman splitting measured with the $\pi/2 - \tau - \pi - \tau - \pi/2$ sequence and the splitting measured with the $\pi/2 - 100 \text{ ms} - \pi$ sequence. In this way a complete decay of echo corresponds to $\sim 0 \mu\text{eV}$ signal. For Rabi-oscillations measurements we subtract the Zeeman splitting obtained from a measurement with a single $\pi/2$ pulse.

The total duration of stages 2 – 4 does not exceed $\sim 2 \text{ s}$, which is much shorter than the nuclear spin polarization longitudinal (T_1) decay time ($>1 \text{ hour}$). In order to improve the signal to noise ratio the experimental cycle is repeated 10 – 50 times during the photoluminescence spectrum acquisition for each parameter value [e.g. for each value of 2τ in the spin echo measurements].

B. Pulsed optically detected NMR: the hardware

A schematic circuit diagram of the NMR setup is shown in Fig. S2(a). The "chirp" and the "resonant" pulses are generated in separate arms, each containing a digital arbitrary/function

generator, a high power amplifier and a matching network. The signal from one of the two arms is selected by a mechanical relay and is then transmitted into the low temperature vacuum insert via a coaxial cable. All equipment and cables have $50\ \Omega$ impedance, while the coil impedance differs significantly from $50\ \Omega$, hence the need for the matching networks. For resonant NMR pulses only a narrow bandwidth is required (few hundred kHz); thus we use a single stub network which gives nearly ideal impedance matching at a specific frequency. The "chirped" pulse requires a much larger bandwidth (up to 20 MHz), over which it is impossible to achieve good impedance matching. In that case the role of the matching network (consisting of lumped LC elements and cables of different length) is to provide nearly constant transmission over the frequency sweep band. The large mismatch of such a network is compensated by the use of a mismatch-tolerant class-A power amplifier.

A schematic drawing of the NMR coil arrangement is shown in Fig. S2(b). The coil consists of 6 turns of a copper wire (diameter 0.4 mm) wound in two layers. The external radius of the coil is smaller than the working distance of the lens used to excite and collect photoluminescence. As a result the coil can be positioned very close to the edge of the quantum dot sample: the distance between the coil edge and the lens focal point is ~ 0.5 mm. The lens and the coil are fixed while the sample is mounted on an XYZ piezo-positioner allowing the sample surface to be scanned and different individual dots to be studied. For the range of frequencies used (5-110 MHz) the coil produces an oscillating magnetic field ~ 20 mT for an input power of 100 W.

S3. ADDITIONAL EXPERIMENTAL RESULTS

All experimental results presented in the main text were measured on the same quantum dot QD1. To verify the consistency of our conclusions we have carried out spin echo decay measurements on an additional set of different dots (QD2-QD7) from the same sample. Spin echo decay curves of ^{75}As measured for dots QD1-QD7 at $B_z = 8$ T are shown in Fig. S3(a) with different colours.

Quantum dots QD1-QD6 demonstrate echo decay that can be well described by a Gaussian function. By contrast, one of the dots (QD7) demonstrates significantly faster non-Gaussian decay.

The echo decay times T_2 obtained from Gaussian fitting are shown in Fig. S3(b) for QD1-QD6. There is some dot-to-dot variation. However, it is comparable to the experimental error, and all of the experimental T_2 values are also in good agreement with the calculated decay time of ~ 4.03 ms, confirming the reproducibility of the presented experimental results and analysis.

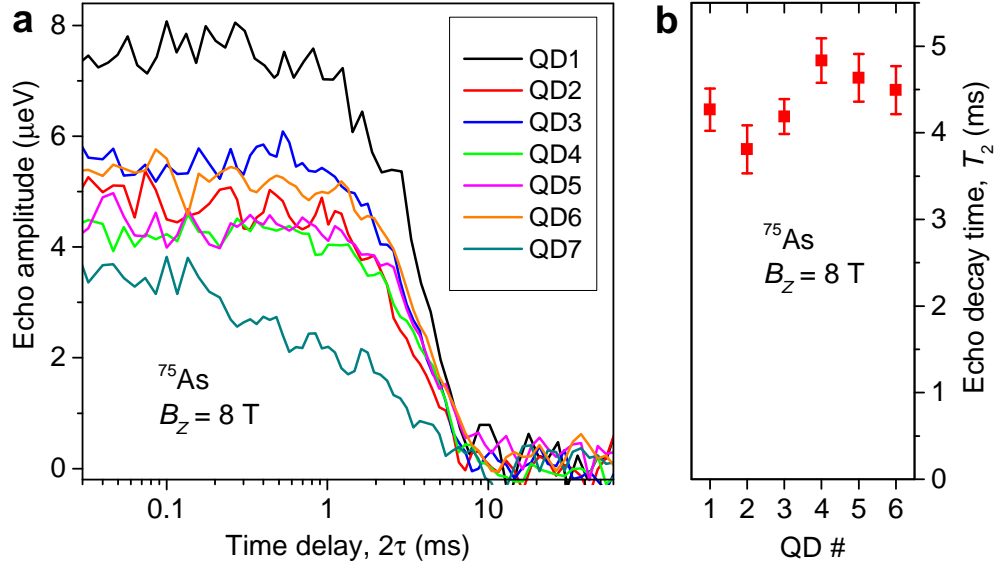


FIG. S3. **Additional echo decay measurements.** **a**, Spin echo decay curves of ^{75}As measured for dots QD1-QD7 at $B_z = 8$ T. **b**, Spin echo decay times T_2 obtained for dots QD1-QD6 using Gaussian fitting of the curves in **a** (90% confidence intervals).

The considerably faster echo decay observed for QD7 is not fully understood. One possibility is that additional nuclear spin decoherence is caused by charge fluctuations. Such fluctuations can not be controlled in our experiments, since we are using electric-gate-free structures. Thus electrons or holes can hop between the nearby impurities or can randomly populate the dot. This might also be the cause for some dot-to-dot variations in T_2 values and will be a subject of further studies (e.g. using dots in Schottky-diode structures).

S4. FIRST PRINCIPLE CALCULATION OF THE NUCLEAR SPIN-ECHO DECAY TIME T_2

Our calculations are done within a framework developed by Haase and Oldfield in Ref.^{S13}. Their model is based on the well-known method of moments initially developed by Van Vleck^{S14}. Below we outline the key points of this model and show how it is used to derive the results presented in the main text.

The decay of the nuclear spin echo is caused by the dipole-dipole interaction between nuclear spins. At sufficiently large magnetic field along Oz (above a few mT) the interaction between two

nuclear spins I and J is described by the "truncated" dipole-dipole Hamiltonian^{S15}:

$$\begin{aligned}\hat{H}_{dd}/(2\pi\hbar) &= \nu_{dd} \left[\hat{I}_z \hat{J}_z - \frac{1}{2}(\hat{I}_x \hat{J}_x + \hat{I}_y \hat{J}_y) \right], \\ \nu_{dd} &= \frac{\mu_0}{4\pi} \frac{\hbar}{2\pi} \gamma_I \gamma_J \frac{1 - 3 \cos^2 \theta}{r^3},\end{aligned}\tag{S1}$$

where \hat{I} and \hat{J} are the nuclear spin operators, and ν_{dd} is the coupling strength. ν_{dd} depends on the gyromagnetic ratio γ_I (γ_J) of the spin I (J), the internuclear distance r and the angle θ between the magnetic field and the vector \vec{r} connecting the nuclei ($\nu_{dd} \lesssim 200$ Hz in frequency units for all nuclei in InGaAs sample).

The interactions between nuclei of the same type (homonuclear coupling) and the nuclei of different types (heteronuclear coupling) have a different role in nuclear spin echo decay. The dephasing caused by the homonuclear coupling is not refocused by the π pulse and, as a result, the spin echo decays. The heteronuclear coupling between the "studied" spins of isotope I and the spins of "another" isotope S , can be viewed as a randomly distributed magnetic field induced by isotope S and acting on I . On sufficiently short time-scales this effective field is static and thus its effect is refocused by the π pulse. However, the spin flip-flops induced by the homonuclear coupling of the S nuclei will make this effective magnetic field time-dependent. As a result the spin echo of isotope I will decay via the spectral diffusion mechanism (this is exactly the same mechanism that causes the decoherence of the electron spin interacting with the nuclear spin bath^{S16-S18}). Below we will consider both homonuclear and heteronuclear interaction.

Quadrupolar interactions modify nuclear spin spectra and affect nuclear spin dephasing dynamics (for introduction to quadrupolar effects see Chapter X of Ref.^{S19}). An exact treatment of nuclear spin echo decay under the combined effect of quadrupolar and dipole-dipole Hamiltonians is unattainable. However, the echo decay times can be obtained relatively easily for two limiting cases^{S13}: (i) The quadrupolar interaction is strongly inhomogeneous, i.e. the difference in quadrupolar shifts (including the second-order shifts) of the nearby nuclei is much larger than their dipolar coupling. Under these conditions all dipolar nuclear flip-flops are energetically forbidden. Such a case would correspond to a self-assembled quantum dot where first-order quadrupolar shifts are strongly inhomogeneous due to inhomogeneous elastic strain, while second-order shifts are inhomogeneous due to atomic-scale disorder. (ii) The opposite case is observed for homogeneous quadrupolar interactions, i.e. each nucleus of a particular isotope is subject to the same electric field gradient. In that case the flip-flops between nuclear spins I and J of the type $(I_z = m, J_z = m \pm 1) \leftrightarrow (I_z = m \pm 1, J_z = m)$ are energetically allowed. This case is relevant for uniformly strained GaAs/AlGaAs quantum wells^{S20-S22}. We now consider these two cases

in detail.

A. Nuclear spin echo decay under strongly inhomogeneous quadrupolar shifts [case (i)].

This case is the easiest for numerical calculations. Since all flip-flops are forbidden, the only source of nuclear spin echo decay is due to the diagonal ($\hat{I}_z \hat{J}_z$) part of the homonuclear dipole-dipole interaction (heteronuclear coupling has no effect since there are no flip-flops that can cause spectral diffusion).

The nuclear spin echo decay time T_2 (the time during which the echo amplitude decays to $1/e$ of its initial value) due to the homonuclear coupling can be approximated as^{S13}:

$$T_2 = \sqrt{2/M_{2E}}, \quad (\text{S2})$$

where M_{2E} is the second moment of the dipole-dipole interaction (Hamiltonian Eq. S1) calculated for the whole crystal:

$$M_{2E} = F \left(\frac{\mu_0}{4\pi} \right)^2 \hbar^2 \gamma^4 a^{-6} \rho \sum_{i \neq 0} \left(\frac{3}{2} \times \frac{1 - 3 \cos^2 \theta_i}{(r_i/a)^3} \right)^2, \quad (\text{S3})$$

where μ_0 is vacuum magnetic permeability (introduced here to carry out calculations in SI units), \hbar - Planck's constant, γ - nuclear gyromagnetic ratio. The summation goes over the whole crystal, r_i is the length of the vector \vec{r}_i between the i -th nucleus and the nucleus chosen as an origin ($i=0$), θ_i is the angle between \vec{r}_i and the direction of magnetic field, a - is the lattice constant. ρ - is the isotope abundance. Here we take into account that all isotopes are sufficiently abundant ($\rho > 0.1$) so that $M_{2E} \propto \rho$ (Chapter IV, §9 of Ref.^{S15}). The factor F depends on the nature of the quadrupolar shifts and the studied transition. For spin-echo decay of the central transition under selective excitation and under strongly inhomogeneous quadrupolar shifts [case (i)] it is:

$$F = \frac{2}{9(2I + 1)}, \quad (\text{S4})$$

The fcc lattice sum is calculated numerically

$$\sum_{i \neq 0} \left(\frac{3}{2} \times \frac{1 - 3 \cos^2 \theta_i}{(r_i/a)^3} \right)^2 \approx 155.13, \quad (\text{S5})$$

Since ^{75}As is the only isotope of arsenic, we have $\rho = 1$. The relative concentration of indium and gallium in the studied dots is estimated to be 0.24 and 0.76 respectively^{S4}. Taking also into account the natural abundances we have $\rho \approx 0.46$ for ^{69}Ga , $\rho \approx 0.30$ for ^{71}Ga and $\rho \approx 0.23$ for ^{115}In . These and other nuclear parameters are listed in Table S1.

TABLE S1. Nuclear spin parameters and calculated nuclear spin echo decay times T_2

Parameter	^{75}As	^{115}In	^{69}Ga	^{71}Ga
Nuclear spin I	3/2	9/2	3/2	3/2
Gyromagnetic ratio γ ($10^7 \text{ s}^{-1}/\text{T}$)	4.596	5.897	6.439	8.181
Natural abundance	1	0.957	0.601	0.399
Abundance in studied quantum dots ρ	1	0.23	0.46	0.3
Calculated T_2 times (ms) for the studied dots:				
Strongly inhomogeneous quadrupolar shifts. $T_{2,zz}$	4.03	8.08	3.04	2.31
Homogeneous quadrupolar shifts. $T_{2,zz+ff}$	1.3	0.55	0.98	0.75
Homogeneous quadrupolar shifts, including the effect of heteronuclear couplings. $T_{2,zz+ff+IS}$	0.93	0.42	0.66	0.51

The low temperature lattice constant of GaAs is $a_0 = 0.564786 \text{ nm}$. The lattice constant of bulk InAs is larger by 7.17%. To take into account that only 24% of atoms are indium we use linear interpolation of lattice constant dependence on indium concentration. Furthermore the lattice constant is modified by the elastic strain. To estimate this effect we first need to imagine that an InGaAs dot is uniformly compressed to match the lattice constant of GaAs and is embedded into the unstrained GaAs matrix in a defect-free manner^{S23}. Such structure is not in equilibrium - the strain fields have to relax resulting in quantum dot expansion. Theoretical analysis shows that a strained InGaAs dot recovers $\sim 2/3$ of the changes in size that were initially induced by compression^{S23}. Thus for the lattice constant we use the following estimate $a \approx a_0(1 + \frac{2}{3} \times 0.24 \times 0.0717) \approx 0.571 \text{ nm}$.

Using these values we calculate the following echo decay times for case (i) which we denote as $T_{2,zz}$: 4.03 ms for ^{75}As , 3.04 ms for ^{69}Ga , 2.31 ms for ^{71}Ga and 8.08 ms for ^{115}In . These $T_{2,zz}$ values are also given in Table S1 and are shown by the solid lines in Fig. 3 of the main text.

B. Nuclear spin echo decay under homogeneous quadrupolar shifts [case (ii)].

Nuclear spin echo decay in case (ii) is caused by both homonuclear and heteronuclear dipole-dipole couplings. First we consider the homonuclear interaction: now in addition to the diagonal part ($\propto \hat{I}_z \hat{J}_z$), the flip-flop part ($\propto \hat{I}_x \hat{J}_x + \hat{I}_y \hat{J}_y$) of the Hamiltonian eq. S1 also contributes to echo decay. This is taken into account by using a different value of F in eq. S3 which now reads^{S13}:

$$F = \frac{2}{9(2I+1)} \times \frac{80I^4 + 160I^3 + 344I^2 + 264I + 333}{256}. \quad (\text{S6})$$

The resulting echo decay times (which we denote as $T_{2,zz+ff}$) are 1.3 ms for ^{75}As , 0.98 ms for ^{69}Ga , 0.75 ms for ^{71}Ga and 0.55 ms for ^{115}In (see also Table S1).

It follows from Eqns. S2, S4, S6 that the ratio of homonuclear decay times in case (i) and case (ii) depends only on spin I : $T_{2,zz}/T_{2,zz+ff} \approx 3.1$ for $I = 3/2$ and $T_{2,zz}/T_{2,zz+ff} \approx 14.8$ for $I = 9/2$. We also note here that the factor F determining the echo decay of the central transition is most influenced by the inhomogeneity of the second-order quadrupolar shifts. By contrast the nature of the first-order quadrupolar shifts makes little difference: values of F differing by less than 10% from that of Eq. S6 can be derived for situations when (a) quadrupolar effects are zero, (b) both first and second order quadrupolar effects are homogeneous, (c) first order effects are inhomogeneous, while second order effects are homogeneous^{S13,S24}. Thus very similar echo decay times are expected for bulk GaAs, uniformly strained and strain-free GaAs/AlGaAs quantum wells.

In order to characterize the timescales of the nuclear flip-flops we introduce the flip-flop time as (Eq. 2 of the main text):

$$T_{2,ff} = 1/(T_2^{-1} - T_{2,zz}^{-1}), \quad (\text{S7})$$

where T_2 is the experimentally measured echo decay time. When homonuclear flip-flops are strongly suppressed, $T_2 \rightarrow T_{2,zz}$ according to the analysis for case (i), so that $T_{2,ff} \rightarrow \infty$ according to Eq. S7. To estimate the $T_{2,ff}$ in the absence of inhomogeneous quadrupolar effects we use the same Eq. S7 but with the calculated $T_{2,zz+ff}$ instead of experimental T_2 . The resulting $T_{2,ff}$ values are 1.5 ms, 1.1 ms and 0.6 ms for ^{69}Ga , ^{71}Ga and ^{115}In respectively (these values are also quoted in the main text).

We now also include the effect of heteronuclear dipole-dipole interaction which causes additional echo decay via spectral diffusion. This effect can not be treated exactly, but it is possible to obtain a reasonable estimate.

First we estimate the root mean square amplitude of the effective field that the "fluctuating" isotope S exerts on the "studied" isotope I . For that we calculate the heteronuclear interaction second moment:

$$M_{2E,S} = F \left(\frac{\mu_0}{4\pi} \right)^2 \hbar^2 \gamma_I^2 \gamma_S^2 a^{-6} \rho_S \sum_{i \neq 0} \left(\frac{3}{2} \times \frac{1 - 3 \cos^2 \theta_i}{(r_i/a)^3} \right)^2$$

$$F = \frac{2}{9(2S+1)}, \quad (\text{S8})$$

where I and S indices denote the values of the corresponding isotopes. In the lattice sum the summation now goes either over the same fcc sublattice (e.g. for interaction between In and Ga),

which gives the same value as in Eq. S5, or over the "other" sublattice (for interaction of As with In or Ga), which gives a lattice sum of ≈ 113.30 .

The echo decay time of the I isotope will depend both on the coupling strength (characterized by $M_{2E,S}$) and the correlation time τ of the flip-flops of the S nuclei. The fastest decoherence of the I nuclei will take place when $\tau \times \sqrt{M_{2E,S}} \sim 1$. Using a Gaussian approximation^{S25} an upper bound on the decay rate under these conditions can be estimated as $\sim \sqrt{M_{2E,S}}/1.62$, where the 1.62 factor is a root of a transcendental equation derived in Ref.^{S25} under the assumption of an exponential correlation function. The overall spin echo decay time of the I nuclei can then be calculated as

$$T_{2,zz+ff+IS} = \left(T_{2,zz+ff}^{-1} + \sum_{S \neq I} \sqrt{M_{2E,S}}/1.62 \right)^{-1}, \quad (\text{S9})$$

where the summation goes over all isotopes S distinct from I . The T_2 times calculated according to Eq. S9 are given in the last row of Table S1 and are also shown by the dashed lines in Fig. 3 of the main text. These estimates are based on the maximum possible effect of the heteronuclear coupling. However, comparing them to the $T_{2,zz+ff}$ values we see that the heteronuclear interaction reduces T_2 times by no more than 40%. Thus the key role in nuclear spin echo decay (and corresponding reduction of T_2) is played by the homonuclear flip-flops.

In these calculations of $T_{2,zz+ff+IS}$ we take into account only the flip-flops of the $S_z = \pm 1/2$ states and the same chemical composition (same values of ρ) as for the studied dots, which corresponds to a hypothetical quantum dot where first-order quadrupolar shifts are strongly inhomogeneous, while second-order shifts are homogeneous or absent. In real self-assembled dots the first-order shifts are strongly inhomogeneous, but the flip-flops of the $\pm 1/2$ states may be suppressed only partially and to a different degree for different isotopes. Thus we may have an intermediate case between cases (i) and (ii), making exact calculation of the nuclear T_2 difficult. But as demonstrated above, one can obtain both the upper and lower bounds on T_2 : $T_{2,zz+ff+IS} < T_2 < T_{2,zz}$.

The observation of $T_2 \approx T_{2,zz}$ for ^{75}As nuclei in strained dots is then interpreted as strong suppression of the homonuclear flip-flops due to strongly inhomogeneous second-order quadrupolar shifts of arsenic (resulting from atomic-scale alloy disorder). By contrast for Ga and In isotopes $T_2 < T_{2,zz}$ is observed in strained dots, implying weaker suppression of the homonuclear flip-flop due to smaller second-order shifts.

Previously the T_2 values calculated using the technique of Ref.^{S13} were shown to deviate by less than 25% from the experimental values^{S13}. As expected the values of $T_{2,zz+ff+IS}$ calculated in the present work are in good agreement with earlier spin-echo decay measurements on ^{75}As

[Refs.^{S20–S22}] and ^{71}Ga [Refs.^{S26,S27}] in lattice matched quantum wells and dots (see triangles in Fig. 3 of the main text) where second-order quadrupolar effects are negligible. Somewhat faster than predicted decay of the ^{71}Ga echo [Refs.^{S26,S27}] was possibly due to the non-selective nature of the measurements resulting in additional echo decay due to residual first-order quadrupolar shifts.

-
- S1. Daraei, A., Tahraoui, A., Sanvitto, D., Timpson, J. A., Fry, P. W., Hopkinson, M., Guimares, P. S. S., Vinck, H., Whittaker, D. M., Skolnick, M. S., and Fox, A. M., Control of polarized single quantum dot emission in high-quality-factor microcavity pillars. *Appl. Phys. Lett.* **88**, 051113 (2006).
 - S2. Sanvitto, D., Daraei, A., Tahraoui, A., Hopkinson, M., Fry, P. W., Whittaker, D. M., and Skolnick, M. S., Observation of ultrahigh quality factor in a semiconductor microcavity. *Appl. Phys. Lett.* **86**, 191109 (2005).
 - S3. Puebla, J., Chekhovich, E. A., Hopkinson, M., Senellart, P., Lemaitre, A., Skolnick, M. S., and Tartakovskii, A. I., Dynamic nuclear polarization in InGaAs/GaAs and GaAs/AlGaAs quantum dots under nonresonant ultralow-power optical excitation. *Phys. Rev. B* **88**, 045306 (2013).
 - S4. Chekhovich, E. A., Kavokin, K. V., Puebla, J., Krysa, A. B., Hopkinson, M., Andreev, A. D., Sanchez, A. M., Beanland, R., Skolnick, M. S., and Tartakovskii, A. I., Structural analysis of strained quantum dots using nuclear magnetic resonance. *Nature Nanotech.* **7**, 646–650 (2012).
 - S5. Chekhovich, E. A., Glazov, M. M., Krysa, A. B., Hopkinson, M., Senellart, P., Lemaitre, A., Skolnick, M. S., and Tartakovskii, A. I., Element-sensitive measurement of the hole-nuclear spin interaction in quantum dots. *Nat. Phys.* **9**, 74–78 (2013).
 - S6. Gammon, D., Efros, A. L., Kennedy, T. A., Rosen, M., Katzer, D. S., Park, D., Brown, S. W., Korenev, V. L., and Merkulov, I. A., Electron and nuclear spin interactions in the optical spectra of single GaAs quantum dots. *Phys. Rev. Lett.* **86**, 5176–5179 (2001).
 - S7. Tartakovskii, A. I., Wright, T., Russell, A., Fal’ko, V. I., Van’kov, A. B., Skiba-Szymanska, J., Drouzas, I., Kolodka, R. S., Skolnick, M. S., Fry, P. W., Tahraoui, A., Liu, H.-Y., and Hopkinson, M., Nuclear spin switch in semiconductor quantum dots. *Phys. Rev. Lett.* **98**, 026806 (2007).
 - S8. Lai, C. W., Maletinsky, P., Badolato, A., and Imamoglu, A., Knight-field-enabled nuclear spin polarization in single quantum dots. *Phys. Rev. Lett.* **96**, 167403 (2006).
 - S9. Eble, B., Krebs, O., Lemaitre, A., Kowalik, K., Kudelski, A., Voisin, P., Urbaszek, B., Marie, X., and Amand, T., Dynamic nuclear polarization of a single charge-tunable InAs/GaAs quantum dot. *Phys. Rev. B* **74**, 081306 (2006).
 - S10. Braun, P.-F., Urbaszek, B., Amand, T., Marie, X., Krebs, O., Eble, B., Lemaitre, A., and Voisin, P., Bistability of the nuclear polarization created through optical pumping in $\text{In}_{1-x}\text{Ga}_x\text{As}$ quantum dots. *Phys. Rev. B* **74**, 245306 (2006).
 - S11. Chekhovich, E. A., Krysa, A. B., Skolnick, M. S., and Tartakovskii, A. I., Light-polarization-

- independent nuclear spin alignment in a quantum dot. *Phys. Rev. B* **83**, 125318 (2011).
- S12. Haase, J. and Conradi, M. S., Sensitivity enhancement for NMR of the central transition of quadrupolar nuclei. *Chemical Physics Letters* **209**, 287 – 291 (1993).
- S13. Haase, J. and Oldfield, E., Spin-echo behavior of nonintegral-spin quadrupolar nuclei in inorganic solids. *Journal of Magnetic Resonance, Series A* **101**, 30 – 40 (1993).
- S14. Van Vleck, J. H., The dipolar broadening of magnetic resonance lines in crystals. *Phys. Rev.* **74**, 1168–1183 (1948).
- S15. Abragam, A., *The principles of Nuclear Magnetism*. Oxford University Press, London (1961).
- S16. de Sousa, R. and Das Sarma, S., Theory of nuclear-induced spectral diffusion: Spin decoherence of phosphorus donors in Si and GaAs quantum dots. *Phys. Rev. B* **68**, 115322 (2003).
- S17. Witzel, W. M. and Das Sarma, S., Quantum theory for electron spin decoherence induced by nuclear spin dynamics in semiconductor quantum computer architectures: Spectral diffusion of localized electron spins in the nuclear solid-state environment. *Phys. Rev. B* **74**, 035322 (2006).
- S18. Yao, W., Liu, R.-B., and Sham, L. J., Theory of electron spin decoherence by interacting nuclear spins in a quantum dot. *Phys. Rev. B* **74**, 195301 (2006).
- S19. Slichter, C. P., *Principles of Magnetic Resonance, Third Edition*. Springer-Verlag, Berlin (1989).
- S20. Kondo, Y., Ono, M., Matsuzaka, S., Morita, K., Sanada, H., Ohno, Y., and Ohno, H., Multipulse operation and optical detection of nuclear spin coherence in a GaAs/AlGaAs quantum well. *Phys. Rev. Lett.* **101**, 207601 (2008).
- S21. Ono, M., Sato, G., Ishihara, J., Matsuzaka, S., Ohno, Y., and Ohno, H., Nuclear spin coherence time in a strained GaAs quantum well. *AIP Conference Proceedings* **1399**, 685–686 (2011).
- S22. Ishihara, J., Ono, M., Sato, G., Matsuzaka, S., Ohno, Y., and Ohno, H., Magnetic field dependence of quadrupolar splitting and nuclear spin coherence time in a strained (110) GaAs quantum well. *Japanese Journal of Applied Physics* **50**, 04DM03 (2011).
- S23. Davies, J. H., Elastic and piezoelectric fields around a buried quantum dot: A simple picture. *Journal of Applied Physics* **84**, 1358–1365 (1998).
- S24. Kambe, K. and Ollom, J. F., Dipolar broadening of the central line of a magnetic resonance for half-integral spin. *Journal of the Physical Society of Japan* **11**, 50–52 (1956).
- S25. Recchia, C. H., Gorny, K., and Pennington, C. H., Gaussian-approximation formalism for evaluating decay of NMR spin echoes. *Phys. Rev. B* **54**, 4207–4217 (1996).
- S26. Sanada, H., Kondo, Y., Matsuzaka, S., Morita, K., Hu, C. Y., Ohno, Y., and Ohno, H., Optical pump-probe measurements of local nuclear spin coherence in semiconductor quantum wells. *Phys. Rev. Lett.* **96**, 067602 (2006).
- S27. Makhonin, M. N., Kavokin, K. V., Senellart, P., Lemaitre, A., Ramsay, A. J., Skolnick, M. S., and Tartakovskii, A. I., Fast control of nuclear spin polarization in an optically pumped single quantum dot. *Nature Materials* **10**, 848 (2011).